Iranica Journal of Energy & Environment 3 (1): 105-113, 2012
ISSN 2079-2115
IJEE an Official Peer Reviewed Journal of Babol Noshirvani University of Technology
DOI: 10.5829/idosi.ijee.2012.03.01.3096

BUT

The Numerical Investigation on Vortex Flow Behavior Using FLOW-3D

Jafar Chapokpour, Firouz Ghasemzadeh and Javad Farhoudi

Department of Irrigation Engineering, Faculty of Agricultural Technology
and Engineering, UTCAN, University of Tehran, Iran

(Received: October 26, 2011; Accepted: November 28, 2012)

Abstract: In this paper a numerical investigation is given for a Rankine type vortex flow inside the cylindrical vortex chamber using FLOW-3D. The FLOW-3D is a general purpose computational fluid dynamics (CFD) package. The fluid motion is described with non-linear, transient, second-order differential equations. Additionally the free surface also exists in many simulations carried out with FLOW-3D because flow parameters and materials properties, such as density, velocity and pressure experience a discontinuity at it. After analysis of the vortex by mentioned details, the finding of time-averaged velocity components, turbulent components, turbulence dissipation, in the 2D briefed sections of chamber were depicted. It was found that there are different flow patterns like clockwise/anticlockwise vortices and some sink points combined with each other in different time intervals, decaying and generating along the time. Also the turbulence intensity and dissipations around the boundary conditions of chamber like central flushing discharge are higher than the flow body. It was also found that this CFD package was not able to simulate thoroughly the central air core of chamber after filling of chamber. This analysis is validated by comparison with previous experimental data that was measured in vortex settling basin.

Key words: Vortex flow · Flow 3D · Numerical Investigation · Turbulence

INTRODUCTION

A vortex-settling basin (VSB) is a fluidic device that uses only the vortices of the flow to extract the bed and suspended loads in the inlet canal. The size of a VSB is very small, compared with conventional settling basins treating the same volume of water and sediment load [1]. Thus the cost of construction of a VSB is just a fraction of the cost required for the construction of a classical settling basin to extract comparable particles [2]. The VSB structure holds promise as an economical, efficient and water-conserving alternative to the other available sediment extraction devices. To remove sediment, a VSB utilizes the secondary flow generated by the circulatory flow induced in a circular basin of diameter. The secondary flow develops as a result of: (a) The deceleration of bottom layers of the fluid by friction between the basin floor and the fluid; and (b) cross-flow currents [3]. Maximization of the strength of circulation should be warranted by placing the basin tangentially to the inlet canal. The secondary flow moves the fluid layers near the basin floor toward the orifice of the flushing pipe, installed at the center of the basin. Sediment particles heavier than the fluid are thus moved along spiral paths from the basin periphery toward the orifice, to be eventually flushed out into a waste channel and conveyed to some natural drainage, as is done in the case of other sediment-extraction devices. The air core developing at the center of the orifice reduces the flushing discharge. The trajectories described by sediment particles make their settling lengths many times longer than the basin diameter, thereby permitting higher inlet velocities compared with conventional settling basins. Because of the single-inlet port, the axis of the air core makes a small angle with the vertical and is slightly displaced with respect to the center of the orifice [4]. The understanding of the phenomenon of settling in a vortex basin requires knowledge of the mechanics of fluid flow and particle flow.

It is well known that when flow enters tangentially into a circular basin with an axial outlet pipe at its center, it is set into circulatory motion with respect to the vertical axis through the center of basin. Experimental studies by Cecen and Akmandor [5] and Cecen and Bayazit [6]

Corresponding Author: Jafar Chapokpour, Department of Irrigation and Reclamation Engineering, University of Tehran, Karaj, Iran. Fax: +982612231787.

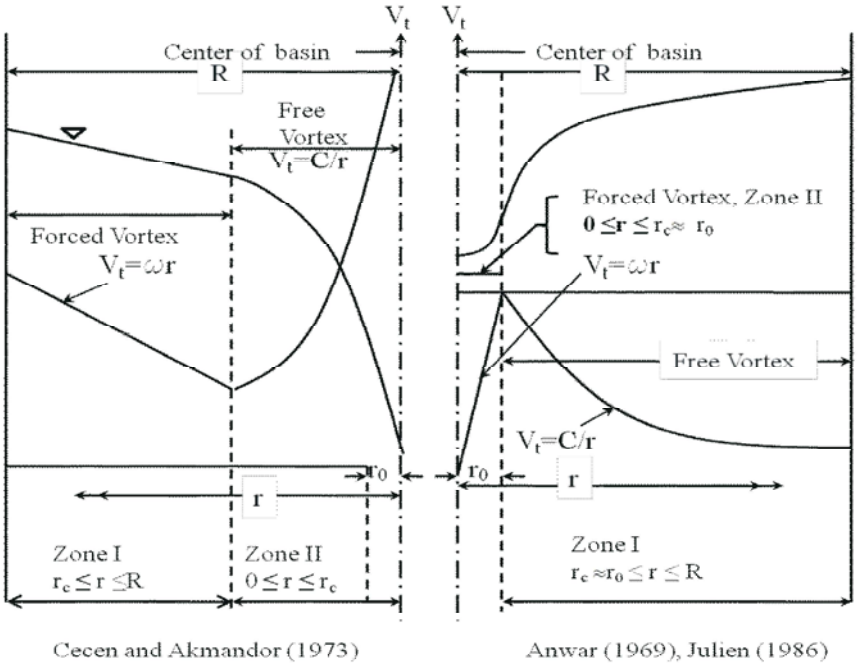

Fig. 1: Flow characteristics in vortex settling basin

show that the circulatory motion generates: (1) A forced vortex in the outer region, i.e., zone I, $r_c<r<R$; and (2) a free vortex in the inner region, i.e., zone II, $0 < r < r_c$, as shown in Fig. 1(a). Here, r is the radial distance from the center of basin or orifice, R is the radius of circular basin, r_0 is the radius of flushing pipe and r_c is the distance (from the center of basin) to the intersection of the forced and free vortices. Mashauri [7] indicated that the forced vortex extends in the region r = 0.33R to R and the free vortex in the region r = 0 to 0.33R, i.e., the two vortices intersect at a distance r_c = 0.33R. According to Anwar [8], the circulatory motion produces a Rankine combined vortex comprising: (1) A forced-vortex core in the inner region, r = 0 to r_0, where, in a relatively small central portion, fluid rotates as a highly viscous solid body; and (2) a non-viscous free vortex in the region, r = r_0 to R, i.e., extending radialy outward from the forced-vortex core. It will be shown later that the Rankine combined vortex theory is appropriate to describe the settling phenomenon in a VSB [1]. The present study aims to investigate the three-dimensional turbulent flow field in the cylindrical vortex chamber as a sediment extractor device by numerical investigation using FLOW-3D CFD package. Another experimental velocity measurement also has done using ADV (Acoustic Doppler Velocity Meter) to verify numerical simulation. FLOW-3D is a general purpose computational fluid dynamics (CFD) package. It employs specially developed numerical techniques to solve the equations of motion for fluids to obtain transient, three-dimensional solutions to multi-scale, multi-phases flow problems. An array of physical and numerical options allows users to apply FLOW-3D to a wide variety of fluid flow and heat transfer phenomena. Fluid motion is described with non-linear, transient, second-order differential equations. The fluid equations of motion must be employed to solve these equations. A numerical solution of these equations involves approximating the various terms with algebraic expressions. The resulting equations are then solved to yield an approximate solution to the original problem. Typically, a numerical model starts with a computational mesh, or grid. It consists of a number of interconnected elements, or cells. These cells subdivide the physical space into small volumes with several nodes associated with each such volume. The nodes are used to store values of the unknowns, such as pressure, temperature and velocity. The mesh is effectively the numerical space that replaces the original physical one. It provides the means for defining the flow parameters at discrete locations, setting boundary conditions and, of course, for developing numerical approximations of the fluid motion equations. The FLOW-3D approach is to subdivide the flow domain into a grid of rectangular cells, sometimes called brick elements. A computational mesh effectively discretizes the physical space. Each fluid parameter is represented in a mesh by an array of values at discrete points.

Since the actual physical parameters vary continuously in space, a mesh with a fine spacing between nodes provides a better representation to the reality than a coarser one. We arrive then at a fundamental property of a numerical approximation: any valid numerical approximation approaches the original equations as the grid spacing is reduced. If an approximation does not satisfy this condition, then it must be deemed incorrect [9].

MATERIALS AND METHODS

Experimental Layout and Methodology: The tests were performed in a configuration in which the angular distance of inlet and overflow outlet was 0 degree as recommended by Paul *et al*. [1]. To maintain a tangential inlet flow jet in the vortex basin, a diaphragm was installed across the entrance channel at a level of 0.12m from the canal bed. Water was then supplied from a constant head tank connected through upstream stilling tank to the circulating water supply system of the laboratory where the incoming flow was regulated by means of a turning valve. Precautions were made to avoid large eddies and disturbances at the free surface of water in upstream stilling tank. The discharge from overflow weir and flushing orifice were measured by means of a pre-calibrated sharp crested rectangular weir and a V-notch respectively. The detailed characteristics of physical model is shown in Table 1 and schematically depicted in Figs. 2, 3.

The velocities were measured in eight radial sections at intervals of 45° from the origin, as shown in Fig. 3. At each radial section 56 points were selected in a grid of velocity measurement, resulting in a total of 448 measuring points inside the chamber. The collected velocity data filtered and analyzed then 2D streamlines in the radial and horizontal sections were drawn and then interpreted.

Numerical Layout: There are two key definitions for geometry construction: Components and Subcomponents. Components represent the portions of a given simulation that will share common properties and initial conditions. Components have specific properties that distinguish them from each other. A component may not necessarily be a continuous entity. Subcomponents represent solid objects, holes and complements within a given component. A simulation can have multiple components and each component may consist of multiple subcomponents. Components can be constructed by defining a single subcomponent or, for more complex flow regions, by adding and subtracting a series of subcomponents.

As shown in Fig. 4, in this numerical investigation, the basin was separated to three different zones in grid length. a) The region around basin center simulated by 0.5cm grid distance. b) The region around basin wall and overflowing weir simulated by 1cm grid distance. c) The remained other flow zones simulated by 2cm grid distance.

Table 1: Characteristics of settling basin

Height of chamber H (m)	Diameter of central orifice d_o (m)	Type of overflow weir L_1 (m)	Diameter of chamber d (m)	Basin depth at periphery h_2 (m)	Width of inlet channel B(m)	Length of inlet channel (m)	Slope of inlet channel S %
0.7	0.075	Circular overflow weir with crest length of 0.8	1.5	0.06	0.3	6	0.045

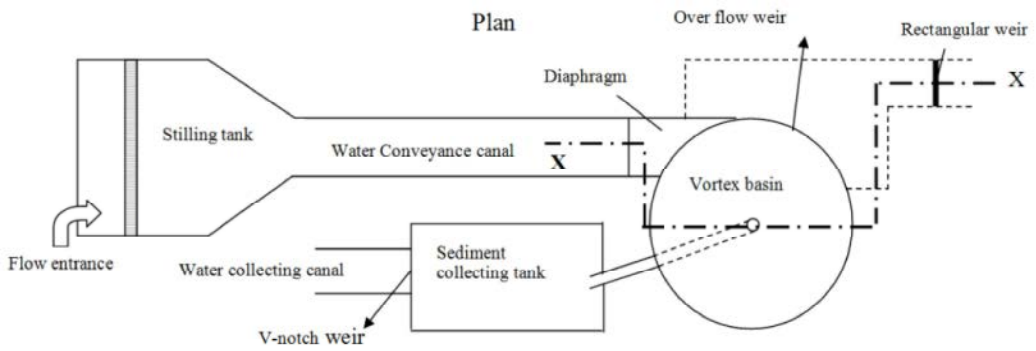

Fig. 2: Schematic layout and parameters of vortex settling basin, Grid of data collection for velocity measurement

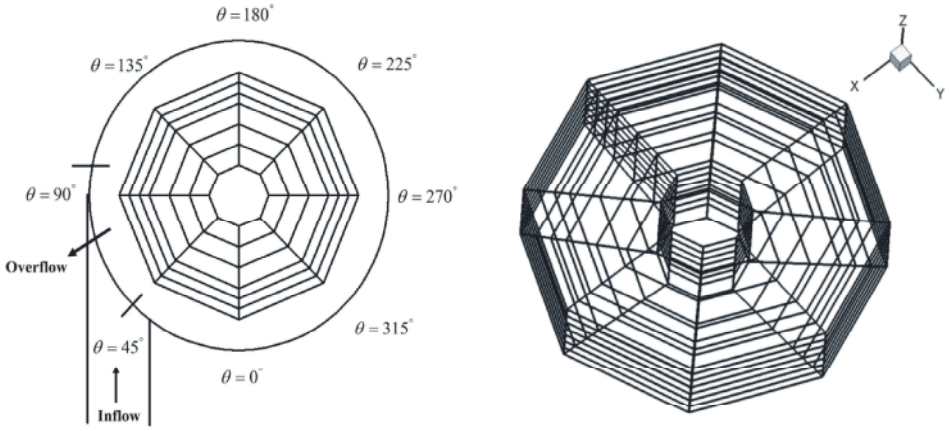

Fig. 3: Grid of data collection for velocity measurement

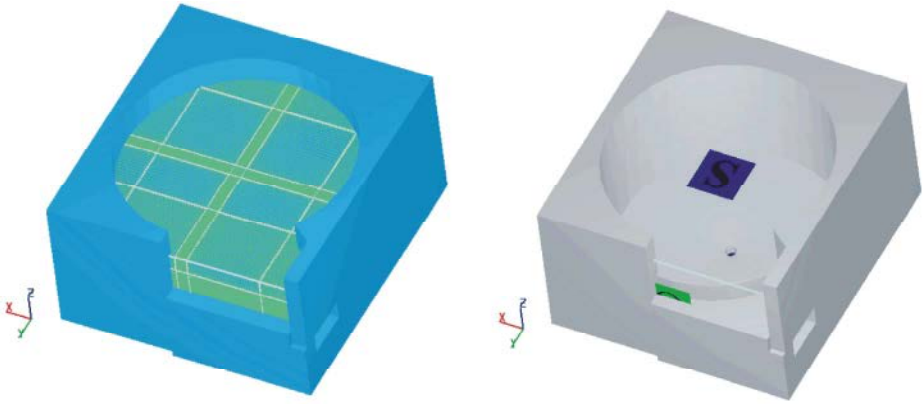

Fig. 4: Numerical mesh and boundary conditions of vortex settling basin

RESULTS AND DISCUSSION

Velocity Vectors and Streamline: Chabokpour [10] has investigated the flow structure of vortex experimentally and observed the different types of flow patterns inside of basin. He concluded that these abovementioned flow patterns have a great influence on hydraulic and removal efficiencies of the basin.

In this study the time averaged velocity distribution in Cartesian coordinate system is represented by (u, v, w) where: u: x direction velocity, v: y direction velocity and w: z direction velocity. Then the velocity vectors and resultant streamlines are depicted by both of these components in radial (XZ, YZ) plane (Figs. 5, 6).

The first notable conclusion is that against laboratory experiments, there is flow body in central

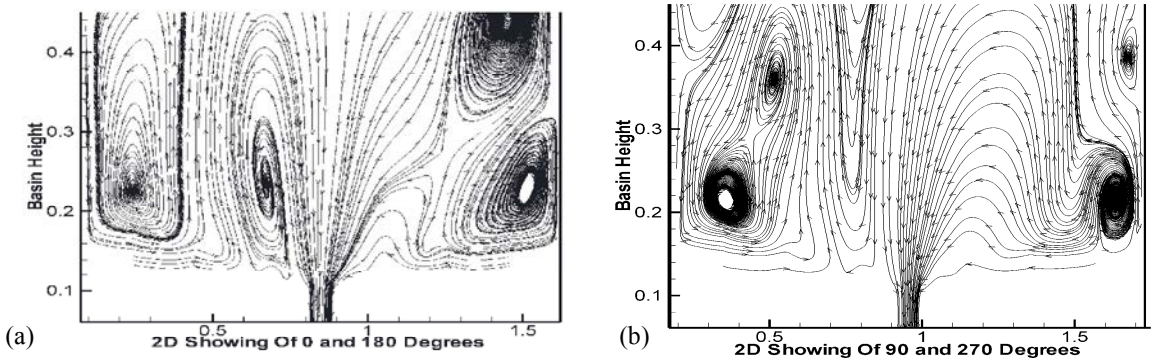

Fig. 5: Detection of streamlines in radial sections of basin at end time of simulation

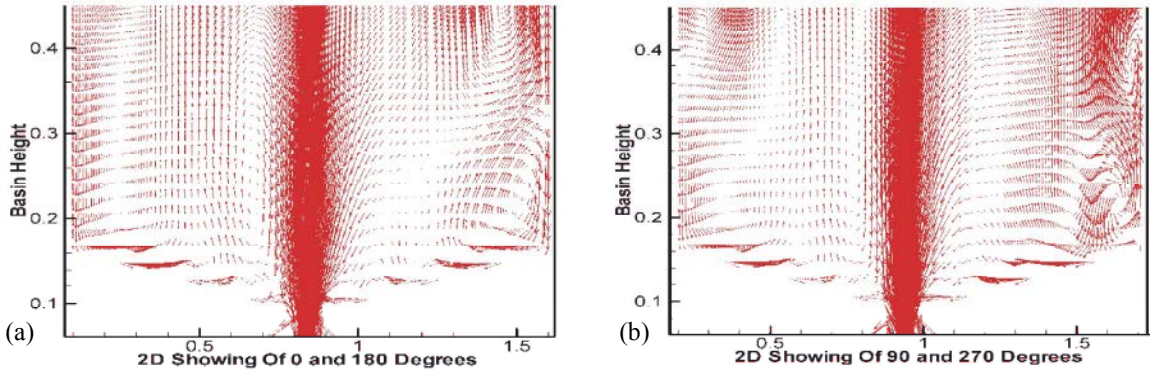

Fig. 6: Detection of velocity vectors in radial sections of basin at end time of simulatio

regions of basin instead of air core. This fact would cause existence of velocity vectors in mentioned regions directing the streamlines towards central flushing orifice. It is also noteworthy to mention that at the beginning time of simulation, the air core was existed but by marching forward in time variable, the central air core was diapered. One of the important numerical techniques in these kind problems is to check grid independency. However, by decreasing of grid length in this area, the FLOW-3D was not able to simulate this region. The air core was existed from beginning of simulation when the basin is filling by the fluid until sidewall weir overflowed.

By precision in Figs. 5, 6, it was found that both clockwise and anti clockwise vortices were produced in four radial sections of basin which would act as effective secondary currents in trapping actions of basin. By comparison between numerical investigation and laboratory findings, it should be mentioned that the shape of created currents in both of them are same. But the position of produced vortices is not completely the same.

At the angle of 0° (Figs. 5a, 6a) that is positioned just before of overflow weir, there are two clockwise and anticlockwise vortices. The anticlockwise vortex is positioned near basin side wall and affected completely by over flow exiting jet. Another vortex (clockwise) is placed just close to basin center having influenced by central flushing orifice.

At the angle of 90° (Figs. 5b, 6b) that is positioned just at the end of overflow weir, the anticlockwise vortex is affected by overflow jet and placed at the end corner of basin wall with a powerful core. The clockwise vortex also weakened by overflow jet, placing its core near to it. At this angle the most direction of streamlines after circulation around powerful anticlockwise vortex is towards central flushing orifice.

At the angle of 180° (Figs. 5a, 6a) that is placed with 180° distance from flow entrance, the direction of near water level vortex changed its direction to anticlockwise, propagating its powerful core with distance from overflow weir. Other near wall vortex also changed its direction to clockwise by the mentioned reason.

At the angle of 270° (Figs. 5b, 6b) that is placed with 90° distance from flow entrance, the vortices affected again with overflow jet, rechanging clockwise vortex's direction to anticlockwise and repositioning at the section.

Turbulence: Turbulence is the chaotic, unstable motion of fluids that occurs when there are insufficient stabilizing forces (i.e., insufficient viscosity). At high Reynolds numbers, the natural instabilities that occur within the flow are not damped out and they manifest in the formation of eddies of various length scales. This behavior is easily observed in flow out of a faucet or in a fast-moving stream by the striations visible on the free surface. Turbulence can be important in industrial processes as well: high pressure die casting filling is most certainly turbulent, as are almost all medium to large scale flow processes.

In FLOW-3D, there are five turbulence models available: the Prandtl mixing length model, the one-equation, the two-equation k-å and RNG models and a large eddy simulation, LES, model. In this investigation, the RNG model, from two equation models was used. At the below some criteria about two-equation k-ε and RNG models were introduced.

Introduction and Formulation: The two-equation turbulence models in FLOW-3D, including the standard and renormalization group (RNG) ε models, are based on the turbulent viscosity hypothesis and solve two transport equations for the turbulent kinetic energy, k and the turbulent dissipation, ε. The RNG k-ε model has several advantages over the standard k-ε

model. It is more accurate for rapidly strained flows and swirling flows and for lower Reynolds numbers (Re), the RNG model behaves better than the standard Ⓚⓔ—ⓔ which is only valid for high Reynolds number flows [11].

The turbulent kinetic energy is defined as the energy of the turbulent velocity fluctuations:

$$k = \frac{1}{2}\left(\overline{u'^2} + \overline{v'^2} + \overline{w'^2}\right) \quad (1)$$

Where u', v' and w' are the components of the velocity fluctuations. Therefore, it can easily be seen that Ⓚ has dimensions of $\frac{L^2}{T^2}$

By definition, the turbulent dissipation is non-negative and has dimensions of $\frac{L^2}{T^3}$.

A length scale can be formed from Ⓚ and Ⓔ as below

$$L_T = \frac{k^{3/2}}{\varepsilon} \quad (2)$$

As well as a time scale

$$T_T = \frac{k}{\varepsilon} \quad (3)$$

Turbulent viscosity can be expressed as the product of the turbulent velocity and length scale. Therefore,

$$v_T \propto \sqrt{k}\frac{k^{3/2}}{\varepsilon} = C_\mu \frac{k^2}{\varepsilon} \quad (4)$$

Where

C_μ = 0.09 in the Ⓚⓔ—ⓔ model and

C_μ = 0.085 in the RNG model.

The transport equation for Ⓚ is

$$\frac{\partial k}{\partial t} + u\frac{\partial k}{\partial x} + v\frac{\partial k}{\partial y} + w\frac{\partial k}{\partial z} = P + G + D_k - \varepsilon \quad (5)$$

Where P is the turbulence production term and in Cartesian coordinates is

$$P = \frac{C_{SP}\mu}{\rho}\left[\begin{array}{l} 2\left(\frac{\partial u}{\partial x}\right)^2 + 2\left(\frac{\partial v}{\partial y}\right)^2 + 2\left(\frac{\partial w}{\partial z}\right)^2 \\ +\left(\frac{\partial v}{\partial x} + \frac{\partial u}{\partial y}\right)^2 + \left(\frac{\partial u}{\partial z} + \frac{\partial w}{\partial x}\right)^2 + \left(\frac{\partial v}{\partial z} + \frac{\partial w}{\partial y}\right)^2 \end{array}\right] \quad (6)$$

Here, C_{SP} is the shear production coefficient. In Eq. (5), G is the buoyancy production term and described as below

$$G = \frac{C_\rho \mu}{\rho^3}\left[\frac{\partial \rho}{\partial x}\frac{\partial p}{\partial x} + \frac{\partial \rho}{\partial y}\frac{\partial p}{\partial y} + \frac{\partial \rho}{\partial z}\frac{\partial p}{\partial z}\right] \quad (7)$$

Where C_P has a default value of 0.0, unless the problem is thermally buoyant, in which case it takes on the value of 2.5. The diffusion term, D_k in Eq. (5) is:

$$D_k = \frac{\partial}{\partial x}\left(\frac{v_T}{\sigma_k}\frac{\partial k}{\partial x}\right) + \frac{\partial}{\partial y}\left(\frac{v_T}{\sigma_k}\frac{\partial k}{\partial y}\right) + \frac{\partial}{\partial z}\left(\frac{v_T}{\sigma_k}\frac{\partial k}{\partial z}\right) \quad (8)$$

Where σ_k = 1.0 in the standard Ⓚⓔ—ⓔ model and σ_k = 0.72 in the RNG Ⓚⓔ—ⓔ model.

The transport equation for Ⓔ is

$$\frac{\partial \varepsilon}{\partial t} + u\frac{\partial \varepsilon}{\partial x} + v\frac{\partial \varepsilon}{\partial y} + w\frac{\partial \varepsilon}{\partial z} = C_{\varepsilon 1}\frac{\varepsilon}{k}\left(P + C_{\varepsilon 3}G\right) + D_\varepsilon - C_{\varepsilon 2}\frac{\varepsilon^2}{k} \quad (9)$$

Where $C_{\varepsilon 1}$, $C_{\varepsilon 2}$ and $C_{\varepsilon 3}$ are user-adjustable, non-dimensional parameters. The default value for $C_{\varepsilon 1}$ is 1.44 for the Ⓚⓔ—ⓔ model and 1.42 for the RNG. $C_{\varepsilon 2}$ Has defaults of 1.92 for the Ⓚⓔ—ⓔ and is computed based on the values of Ⓚ, Ⓔ and the shear rate for the RNG model. $C_{\varepsilon 3}$ has a value of 0.2 for both models. The diffusion term for the dissipation is:

$$D_\varepsilon = \frac{\partial}{\partial x}\left(\frac{v_T}{\sigma_\varepsilon}\frac{\partial \varepsilon}{\partial x}\right) + \frac{\partial}{\partial y}\left(\frac{v_T}{\sigma_\varepsilon}\frac{\partial \varepsilon}{\partial y}\right) + \frac{\partial}{\partial z}\left(\frac{v_T}{\sigma_\varepsilon}\frac{\partial \varepsilon}{\partial z}\right) \quad (10)$$

Where σ_ε = 1.3 in the standard Ⓚⓔ—ⓔ model and σ_ε = 0.72 in the RNG Ⓚⓔ—ⓔ model. In order to prevent unphysically small dissipation rates, the minimum dissipation is limited by a maximum length scale, represented by *TLEN* in FLOW-3D

$$\varepsilon_{\min} = \frac{\sqrt{3/2}C_\mu k^{3/2}}{TLEN} \quad (11)$$

It is recommended to use a value of *TLEN* equal to about 7% of the hydraulic diameter. However, there are often configurations with complex multi-scale features where choosing this parameter is not a straightforward task. It is in those cases where picking a wrong value for *TLEN* may lead to unrealistic results. In FLOW-3D version 9.3 and earlier, specifying *TLEN* was the only option. From Eq. (11), the minimum dissipation then becomes a function only of the local turbulent energy and when this occurs, the two-equation model essentially reverts to a one-equation model.

In FLOW-3D version 9.4, a new option has been incorporated to dynamically compute turbulent length and time scales, Eqs. (2) and (3) and their respective upper and lower bounds which are:

$$L_{T\min} = 70.0\left(\frac{\mu}{\rho}\right)^{3/4}\left(\frac{1}{\varepsilon}\right)^{1/4} \quad (12)$$

$$L_{T\max} = \frac{0.86}{C_\mu}\frac{\sqrt{k}}{S} \quad (13)$$

$$L_{T\min} = 6\sqrt{\frac{\mu}{\rho\varepsilon}} \quad (14)$$

$$L_{T\max} = \frac{0.35}{C_\mu}\frac{1}{S} \quad (15)$$

Where μ is the molecular viscosity, ρ is the density and S is the mean strain rate magnitude computed from the second invariant of the strain tensor.

The lower bounds of the turbulent length and time scales are based on the Kolmogorov scales and the upper bounds are based on the rapid distortion theory. The length scale L_T, Eq. (2), subject to the limits given by Eqs. (12) and (13), is used to limit dissipation:

$$\varepsilon_{\min} = \frac{\sqrt{3/2}C_\mu k^{3/2}}{L_T} \quad (16)$$

The inverse of the time scale T_T, Eq. (3), subject to the limits given by Eqs. (14) and (15), is used on the right-hand side of Eq. (9) where ⍰⍰/⍰⍰ appears. The user still has the option to specify *TLEN* as the constant maximum length scale and bypass the dynamically computed limiters. *TLEN* can also be defined for the turbulent boundary and initial conditions when the option to dynamically compute the bounds is selected. Hereon, we shall refer to *TLEN* as the user-specified, constant maximum length scale and to the new feature as dynamically computed limiters [11].

Computed Turbulence Kinetic Energy: As is shown in Figs. 7, 8, the turbulent kinetic energy (TKE) around central air core has a higher magnitude rather than other zones with maximum of 0.032. It also should be mentioned that by marching upward in basin inside from bed to water surface, a divergence in magnitudes was obtained. Also there are any significant differences between various radial sections. A notable difference between experimental and computational investigations is the more prominent influence of side weir in turbulence creation inside the chamber.

Like TKE parameter, the DTKE (dissipation of turbulence kinetic energy) parameter also in the mentioned region had higher magnitudes rather than other areas. It means that at the positions with higher turbulence, both TKE and DTKE have higher magnitudes.

At the Fig. 8, three horizontal sections were selected to illustrate TKE parameter across the basin height. The selection of sections was in a manner to illustrate the influence of three effecting boundary conditions like basin bed slope, entrance flow jet and overflow jet. As is shown in Fig. 8a, the TKE at the 11cm distance from central orifice is more affected by basin bed slope and the influences of two other effects are negligible. It is also found that the centralization of higher magnitudes was occurred. By marching up to 23cm height from basin center, the influence of entrance jet slowly exhibited, causing more turbulence creation around basin wall. It is also found that the TKE parameter at the basin center had lower magnitudes. Coming up to 35cm distance from basin center, where the overflow weir has started its influence in flow body, the streamlines were directed towards sidewall weir. This phenomenon has introduced the higher magnitudes in TKE and DTKE parameter around the weir and has decreased the concentration of higher magnitudes from basin center. These findings in basin height verify experimental research.

By comparison between experimental and numerical investigations it was also found that in the physical model the measured parameters have a stochastic nature against numerical simulation.

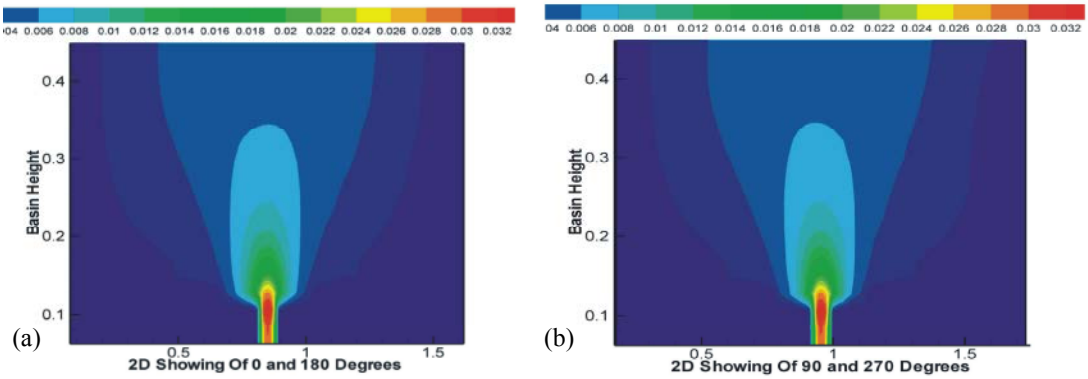

Fig. 7: Computation of (TKE) in radial sections of basin at end time of simulation

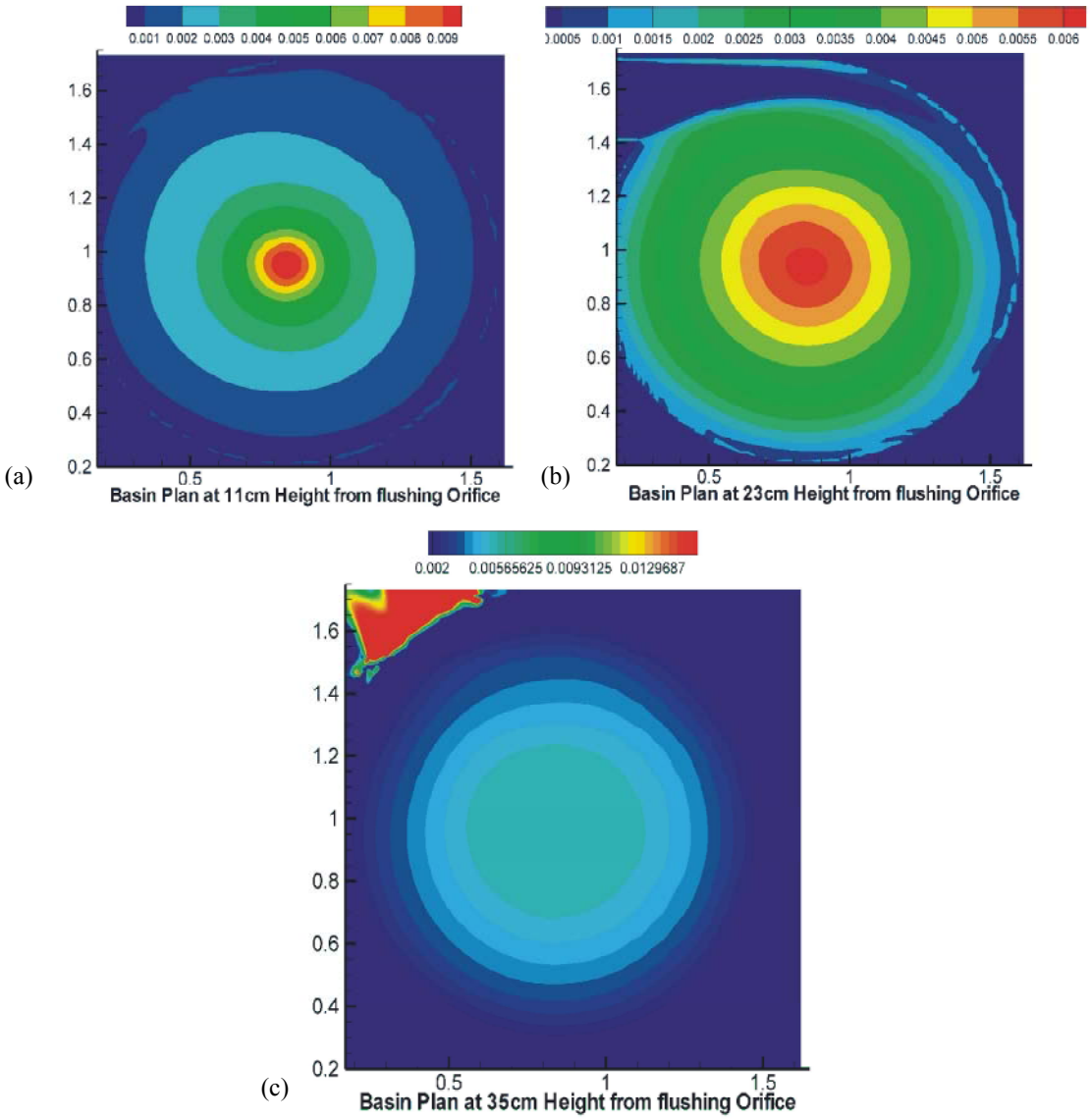

Fig. 8: Computation of (TKE) in horizontal sections of basin at end time of simulation

CONCLUSIONS

Turbulence is the chaotic, unstable motion of fluids that occurs when there are insufficient stabilizing forces (i.e., insufficient viscosity). At high Reynolds numbers, the natural instabilities that occur within the flow are not damped out and they manifest in the formation of eddies of various length scales.

Against laboratory experiments, there is flow body in central regions of basin instead of air core. It is also noteworthy to mention that at the beginning time of simulation, the air core was existed but by marching forward in time variable, the central air core was diapered. One of the important numerical techniques in these kind problems is to check grid indecency. However, by decreasing of grid length in this area, the FLOW-3D was not able again to simulate this region.

Productions of both clockwise and anti clockwise vortices were observed in four radial sections of basin which would act as effective secondary currents in trapping actions of basin. By comparison between numerical investigation and laboratory findings, it should be mentioned that the shape of created currents in both of them are same. But the position of produced vortices is not completely the same.

The kinetic energy around central air core has a higher magnitude rather than other zones. It also should be mentioned that by marching upward in basin inside

from bed to water surface, a divergence in magnitudes was obtained. Also there are any significant differences between various radial sections. A notable difference was observed between experimental and computational investigations in more prominent influence of side weir in turbulence creation. It is also found that in the physical model, the measured parameters have a stochastic nature against numerical simulation.

REFERENCES

1. Paul, T.C., S.K. Sayal, V.S. Sakhanja and G.S. Dhillon, 1991. Vortex settling chamber design considerations. J. Hyd. Engng., 117(2): 172-189.
2. Mashauri, D.A., 1986. Modeling of vortex settling chamber for primary clarification of water. PhD thesis, Tampere University of Technology, Tampere, Finland, pp: 217.
3. Salakhov, F.S., 1975. Rotational design and methods of hydraulic calculation of load-controlling water intake structures for Mountain Rivers. Proceedings of Ninth Congress of the ICID, Moscow, Soviet Union, pp: 151-161.
4. Cecen, K., 1977. Hydraulic criteria of settling basins for water treatment, hydro-power and irrigation. Proc. 17th Congress of the Int. Assoc, of Hydr. Res., BadenBaden, West Germany, pp: 275-294.
5. Cecen, K. and N. Akmandor, 1973. Circular settling basins with horizontal floor. MAG Report No 183, TETAK, Ankara, Turkey.
6. Cecen, K. and M. Bayazit, 1975. Some laboratory studies of sediment controlling structures calculation of load-controlling water intake structures for Mountain Rivers. Proceedings of the Ninth Congress of the ICID, Moscow, Soviet Union, pp: 107-110.
7. Mashauri, D.A., 1986. Modeling of vortex settling chamber for primary clarification of water, PhD thesis, Tampere University of Technology, Tampere, Finland, pp: 217.
8. Anwar, H.O., 1969. Turbulent flow in a vortex. J. Hydr. Res., 7(1): 1-29.
9. http://www.flow3d.com/resources/flow3d-technical-papers-1.html.
10. Chapokpour, J. and J. Farhoudi, 2011. Sediment extraction and flow structure of vortex settling basin. WASJ., 14(5): 782-793.
11. Isfahani, A.H.G. and J.M. Brethour, 2009. On the Implementation of Two-equation Turbulence Models in FLOW-3D, Flow Science, FSI-09-TN86.